Accurate potential energy curves for HeO−, NeO−, and ArO−: Spectroscopy and transport coefficients

Larry A. Viehland, Rhonda Webb, Edmond P.F. Lee, and Timothy G. Wright

Citation: J. Chem. Phys. **122**, 114302 (2005); doi: 10.1063/1.1861874

View online: http://dx.doi.org/10.1063/1.1861874

View Table of Contents: http://jcp.aip.org/resource/1/JCPSA6/v122/i11

Published by the American Institute of Physics.

Accurate potential energy curves for HeO^-, NeO^-, and ArO^-: Spectroscopy and transport coefficients

Larry A. Viehland[a] and Rhonda Webb
Division of Science, Chatham College, Pittsburgh, Pennsylvania 15232

Edmond P. F. Lee[b]
School of Chemistry, University of Southampton, Highfield, Southampton, SO17 1BJ, United Kingdom and Department of Applied Biology and Chemical Technology, Hong Kong Polytechnic University, Hung Hom, Hong Kong

Timothy G. Wright[c]
School of Chemistry, University of Nottingham, University Park, Nottingham, NG7 2RD, United Kingdom

(Received 14 December 2004; accepted 5 January 2005; published online 16 March 2005)

We calculate accurate potential energy curves for HeO^-, NeO^-, and ArO^-, including the full counterpoise correction and allowing for spin–orbit effects. Comparison with previous curves is presented, where these are available. The three curves, $^2\Sigma^+_{1/2}$, $^2\Pi_{1/2}$, and $^2\Pi_{3/2}$, are used to derive spectroscopic constants and to calculate the transport coefficients for O^- moving in a bath of the respective rare gas. Conclusions are made based on a comparison with the available data. © *2005 American Institute of Physics*. [DOI: 10.1063/1.1861874]

I. INTRODUCTION

Over the last five or six years, we have been working on the production of accurate potential energy curves for M^+–Rg species, where M=alkali metal (Li–Fr) and Rg =rare gas (He–Rn). We have now produced accurate potential energy curves for all 36 ion-atom combinations. Initially, the curves were used to produce spectroscopic constants[1–3] but this work expanded into also calculating transport coefficients of M^+ in Rg.[4–7] The latter are a stringent test of a molecular potential when experimental results are known over a wide range of E/N (the ratio of the electric field strength to the gas number density), as the potential then is probed in the short- and long-R regions, as well as near the minimum. In the present work we expand these studies both by moving to systems involving an anion and to one in which two energetically close states are coupled by spin–orbit interaction.

Ab initio calculations have now reached the stage where, for light diatomic molecules (involving first and second row elements), very accurate potential energy curves can be obtained in most cases. This is particularly the case if a single-reference wave function will suffice, for then the CCSD(T) method may be employed (using restricted or unrestricted wave functions) with a moderately large basis set (of quadruple-ζ quality or better, and including polarization functions). For electronegative species and/or anions, diffuse functions must also be included. Complications can arise, however, for open-shell species when spin–orbit coupling must also be considered.

In the present case, when $O^-(^2P)$ is approached by a rare gas atom, $^2\Pi$ and $^2\Sigma^+$ states arise, depending on whether the "hole" lies perpendicular to or along the internuclear axis. These states lie close in energy, and hence the effects of spin–orbit coupling must be considered. The $^2\Pi$ state splits into $^2\Pi_{3/2}$ and $^2\Pi_{1/2}$, and the $\Omega=1/2$ component can interact with the $^2\Sigma^+$ state, which also has $\Omega=1/2$. In principle, all three states may be populated under laboratory conditions, since the spin–orbit splitting in O^- is small at 177.08 cm^{-1} (Ref. 8). We briefly summarize the information available on HeO^-, NeO^-, and ArO^-.

HeO^-. The first study of O^- moving in a rare gas appears to be that of McFarland *et al.* in 1973 (Ref. 9) for the case of helium. In that work, mobilities were measured for a range of E/N at 298 K. (Those data were smoothed and represented by Ellis *et al.* in Ref. 10.) The information was not used to derive any information on the internuclear potential.

In 1977, Lin and Bardsley[11] performed Monte Carlo simulations of the motion of ions drifting though rare gases. The particular case of O^- drifting through helium was considered, and it was noted that a degeneracy is present in the ionic state and that $^2\Sigma^+$ and $^2\Pi$ states needed to be considered. An interaction potential for each state was reported, but it was noted that the derivation of the pair of potentials was "clearly not unique."

Bychov[12] has fitted the mobility data available to an average "O^-–He" potential, but only in a narrow range covering part of the repulsive region ($1.8 \leqslant R \leqslant 2.2$). The form of the potential used was

$$V(r) = U_0 \exp(-\alpha r), \tag{1}$$

where U_0 was determined as 640 eV and α as 3.75 $Å^{-1}$.

More recently, Viggiano, Morris, and Mason measured mobilities of O^- in helium at a range of temperatures[13] from 93 to 563 K. (The data have been smoothed and reported in Ref. 14.) They assumed that there was a statistical split of the interactions into 2/3 for $^2\Pi$ and 1/3 for $^2\Sigma^+$, with the $^2\Pi_\Omega$

[a]Electronic mail: Viehland@chatham.edu
[b]Electronic mail: E.P.Lee@soton.ac.uk
[c]Electronic mail: Timothy.Wright@Nottingham.ac.uk

components also being statistically split in a 1:1 ratio for $\Omega=3/2$ and $1/2$, respectively. (The authors of Ref. 13 noted that it was probable that the statistical weights employed by the authors of Ref. 11 were incorrect, owing to the assumption of a $^2\Pi$ ground state therein.) The potential derived in Ref. 13 from the new mobility data presented therein has a minimum of 5.12 meV (41 cm^{-1}) at 3.53 Å. It was not possible to obtain a separate determination of parameters for more than one potential, and so these parameters correspond to an average O^-–He potential.

NeO^-. As far as we are aware, there is no information available on the potential energy curves, spectroscopy, or transport coefficients for NeO^-.

ArO^-. Bowen and co-workers[15] have reported the results of electron detachment studies of ArO^-. This work was extended in a later study[16] of ArO^- (together with studies on KrO^-, XeO^-, and N_2O^-) that led to dissociation energies and bond lengths for the $^2\Pi$ and $^2\Sigma^+$ states. Prior to that, an *ab initio* study of the photoelectron spectroscopy of ArO^- had been published, in which the low-lying states of ArO^- and ArO were considered;[17] the latter work has also been summarized as part of a review article.[18] In that work $^2\Sigma^+$ and $^2\Pi$ potential energy curves were calculated at various levels of theory with the highest level, UMP4, employing a basis set of triple-ζ quality, augmented with double diffuse functions and also with bond-centered functions, d-aug-cc-pVTZ(+bf). These two potentials were then employed with a model for the spin–orbit coupling [see Eqs. (10) and (11) of Ref. 17], in which the two $\Omega=1/2$ states were allowed to interact. Although spectroscopic parameters were not reported for the spin–orbit curves, standard ion mobilities were reported in graphical form. Also briefly mentioned in that work were some results at the RCCSD(T)/aug-cc-pVQZ(+bf) level. We shall compare the UMP4/d-aug-cc-pVTZ(+bf) potential with our own below.

II. CALCULATIONAL DETAILS

Potential energy curves. Potential energy curves were calculated over a wide range of *R*, covering the long and short regions. The precise range and separations employed were, to some extent, dictated by the demands of the transport coefficient calculations.

RCCSD(T) (Ref. 19) calculations were employed using the MOLPRO package[20] to generate curves for the lowest $^2\Sigma^+$ and $^2\Pi$ states. As noted above, these are the two states that arise as the degeneracy of the ^2P state of O^- is broken by the rare gas atom. The basis sets employed for HeO^- and NeO^- were d-aug-cc-pV5Z. For ArO^-, however, only the singly augmented aug-cc-pV5Z basis set was employed owing to computational limitations. Basis sets were obtained from the Gaussian basis set order form.[21] These curves were point-by-point corrected for basis set superposition error (BSSE), employing the full-counterpoise correction (CP). The frozen-core approximation was employed in all cases except He, which has no core electrons.

Spin–orbit calculations. Spin–orbit coupling was included employing the Breit–Pauli operator, as implemented[22] in MOLPRO. CASSCF calculations are carried out to determine the spin–orbit coupling at each *R*, with the corresponding RCCSD(T) energies being used for the unperturbed states. The CASSCF calculations employed the frozen-core approximation. For the HeO^- calculations, the standard aug-cc-pV5Z basis set was employed for He and O, but only the *s* and *p*, for He, and *s*,*p* and *d* for O were included (uncontracted). For NeO^-, the standard aug-cc-pV5Z basis set was used for Ne and O but only including the *s*, *p*, and *d* functions (uncontracted). For the ArO^- calculations, the aug-cc-pVQZ basis set was used for Ar and O, with only the *s*, *p*, and *d* functions included (uncontracted).

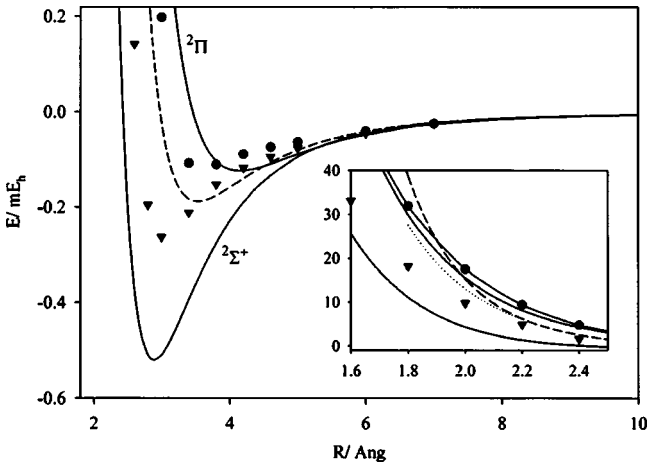

FIG. 1. Comparison of the present counterpoise-corrected RCCSD(T)/d-aug-cc-pV5Z curves for HeO^- $^2\Sigma^+$ and $^2\Pi$ with previously reported curves. The solid lines are the present results; the data points from Ref. 11 are given as inverted triangles ($^2\Sigma^+$) and circles ($^2\Pi$)—note that the state ordering used here is the reverse to that noted in Ref. 11—see text. The dashed line is the 8-6-4 potential from Ref. 13. The same curves are shown in the inset at small internuclear distances, where also the curve from Bychov (Ref. 12) has been included as a dotted line.

Spectroscopy. From the interaction potential energy functions, equilibrium internuclear separations, dissociation energies, and rovibrational energy levels were obtained using LeRoy's LEVEL program.[23]

Transport coefficients. Starting from the interaction potentials, transport cross sections were calculated as a function of ion-neutral collision energy using the program QVALUES.[24,25] Appropriate averages of the cross sections for the $^2\Sigma^+$ and $^2\Pi$ curves, i.e., in the absence of spin–orbit coupling, or for the $^2\Sigma^+_{1/2}$, $^2\Pi_{3/2}$, and $^2\Pi_{1/2}$ curves, i.e., in the presence of spin–orbit coupling, were then taken. In each case, there is an issue as to what ratio of populations of the states to employ, and this will be discussed below.

The average cross sections as a function of collision energy were used in the program GRAMCHAR (Ref. 26) to determine the ion mobility and the other gaseous ion transport coefficients as functions of E/N at particular gas temperatures. The mobilities are generally precise within 0.1%, which means that the numerical procedures within programs QVALUES and GRAMCHAR have converged within 0.1% for the given ion-neutral interaction potential. However, at some intermediate E/N values for NeO^- and ArO^-, convergence is sometimes only within a few tenths of a percent and a slight "wobble" is observed in the computed values. The diffusion coefficients are generally precise within 1%, with the excep-

TABLE I. Spectroscopic data derived for HeO^-.

State	CP	R_e (Å)	D_e (cm^{-1})	D_0 (cm^{-1})	ZPVE	0–1 (cm^{-1})	N_{vib}[a]
$^2\Sigma^+$	No	2.882	119.4	86.8	32.5	44.5	4
$^2\Sigma^+$	Yes	2.892	114.2	82.5	31.7	44.6	4
$^2\Sigma^+_{1/2}$	Yes	2.987	75.0	52.4	22.6	29.0	4
$^2\Pi$	No	4.116	29.0	18.5	10.5	12.0	3
$^2\Pi$	Yes	4.147	27.1	17.1	10.0	12.0	3
$^2\Pi_{3/2}$	Yes	4.146	27.2	17.2	10.0	12.3	3
$^2\Pi_{1/2}$	Yes	3.921	34.1	21.7	12.4	14.8	3

[a]Number of bound vibrational levels.

tion of intermediate E/N values where convergence is only within 3%.

The differences between the measured and calculated transport coefficients were determined graphically and by using statistical quantities, δ and χ, which take into account the estimated errors in each quantity. If the experimental and calculated errors are the same at all E/N, then δ is the ratio of the average percentage difference to the maximum combined percentage difference expected, while χ is the ratio of the standard deviation of the percentage differences to the root mean square of the maximum combined percentage deviations expected. A positive value of δ indicates that the data lie above the calculated values, and vice versa. Values of $|\delta|$ that are substantially lower (alternatively, higher) than 1 indicate that there is substantial agreement (disagreement) between the calculated and measured values, on average. Values of χ that are not much larger than $|\delta|$ indicate that there is little scatter in the experimental data and that the agreement between the calculated and measured values is uniform over all values of E/N, while values of χ substantially greater than $|\delta|$ indicate that at least one of these factors is not true.

III. RESULTS AND DISCUSSION

A. HeO^-

1. Potential energy curves and spectroscopy

First, it has been noted by Viggiano, Morris, and Mason that Lin and Bardsley assigned the lowest state as the $^2\Pi$ state, whereas the former authors deduced that the lowest state was more likely to be a $^2\Sigma^+$ state based upon the known ground state of $HeNe^+$. This state ordering also follows on from considerations based upon the minimization of electron repulsion, and has been discussed for the heavier RgO^- species by de Clercq, Hendricks, and Bowen.[16]

Viggiano, Morris, and Mason fitted their mobility data, obtained over a range of temperatures and a wide range of E/N, to an (n-6-4) potential, which has been put forward for modeling ion-neutral interactions:[27]

$$U^*(r) = \frac{n}{n(3+\gamma) - 12(1+\gamma)} \left\{ \frac{12}{n}(1+\gamma)\left(\frac{r}{r_m}\right)^{-n} - 4\gamma\left(\frac{r}{r_m}\right)^{-6} - 3(1-\gamma)\left(\frac{r}{r_m}\right)^{-4} \right\} \quad (2)$$

where $n=8$, γ was obtained as 0.1, and r_m was found to be 3.53 Å. The well depth obtained was 5.12 meV (41 cm^{-1}), and represents an average of the three spin–orbit states. In Fig. 1 is presented a comparison of the $^2\Sigma^+$ and $^2\Pi$ potential energy curves of Lin and Bardsley, the "averaged" (8-6-4) potential of Viggiano, Morris, and Bowen together with our own CP-corrected RCCSD(T) curves, in the absence of spin–orbit coupling. We also show, in the insert, the repulsive regions of the curves and the potential of Bychov. As may be seen from Fig. 1, we find that the ground state of HeO^- is indeed the $^2\Sigma^+$ state, and that it has a potential well depth significantly deeper than that of the $^2\Pi$ state. In addition, our well depth for the $^2\Sigma^+$ state ($D_0=87$ cm^{-1}) is significantly greater than that of the lowest state of Lin and Bardsley, who obtained well depths of 58 and 26 cm^{-1}. Our $^2\Sigma^+$ well depth is also greater than that of Viggiano, Morris, and Bowen whose averaged potential was only 41 cm^{-1} deep. We note that the value obtained by Viggiano, Morris, and Bowen should perhaps more properly be compared with our $^2\Sigma^+_{1/2}$ value (52.4 cm^{-1}), to which it is much closer (*vide infra*).

Although our HeO^- curves were obtained via an *a priori* correction for BSSE, it is interesting to compare the spectroscopic parameters obtained from the curves both before and after the counterpoise correction is made. Table I presents these spectroscopic parameters. It may be seen that the effect is very small, largely due to the significant internuclear separation in the molecule. Thus, even though O^- might reasonably be expected to lead to basis set superposition effects

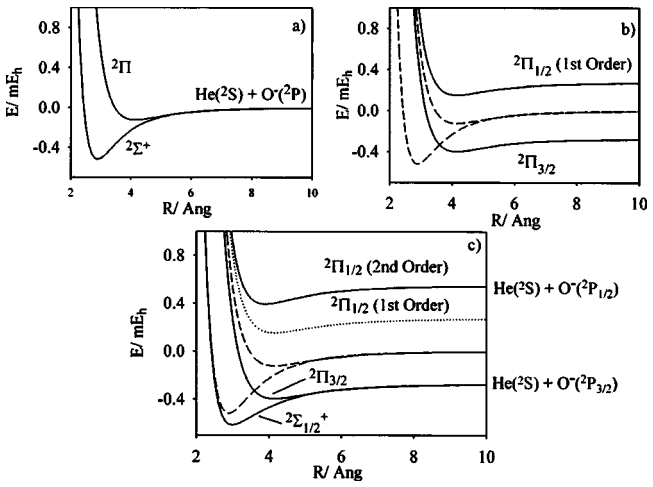

FIG. 2. Counterpoise-corrected RCCSD(T)/d-aug-cc-pV5Z curves for the $^2\Sigma^+$ and $^2\Pi$ states of HeO^- in the (a) absence and (b) presence of spin–orbit coupling in the $^2\Pi$ state. In (c) the subsequent result of the interaction between the $^2\Pi_{1/2}$ and $^2\Sigma^+$ states is shown. See text for details.

TABLE II. Mobility data for HeO^-

Temperature (K) [Ref.]	States considered	Range of E/N	A^a	No.	P^a	δ	χ
93 [13,14]	$^2\Pi$	1.0–12.0	5.0	9	0.1	2.408	2.042
	$^2\Pi_{1/2}$	1.0–12.0	5.0	10		2.079	2.094
	$^2\Pi_{3/2}$	1.0–12.0	5.0	9	0.1	2.024	2.025
	$^2\Sigma^+$	1.0–12.0	5.0	9		2.958	15.493
	$^2\Sigma^+_{1/2}$	1.0–12.0	5.0	10		0.810	1.449
	$^2\Sigma^+/^2\Pi$	1.0–12.0	5.0	9	0.1	2.809	2.848
	$^2\Sigma^+_{1/2}/^2\Pi_{1/2}/^2\Pi_{3/2}$	1.0–12.0	5.0	9	0.05	1.809	1.839
171 [13,14]	$^2\Pi$	1.0–15.0	5.0	10	0.1	0.885	0.887
	$^2\Pi_{1/2}$	1.0–15.0	5.0	10	0.1	0.727	0.728
	$^2\Pi_{3/2}$	1.0–15.0	5.0	10	0.1	0.882	0.884
	$^2\Sigma^+$	1.0–15.0	5.0	10		−0.158	0.828
	$^2\Sigma^+_{1/2}$	1.0–15.0	5.0	10		−2.621	2.639
	$^2\Sigma^+/^2\Pi$	1.0–15.0	5.0	10	0.1	0.639	0.660
	$^2\Sigma^+_{1/2}/^2\Pi_{1/2}/^2\Pi_{3/2}$	1.0–15.0	5.0	10	0.5	−0.015	0.049
300 [9,10]	$^2\Pi$	1.0–160.0	7.0	21		1.090	1.176
	$^2\Pi_{1/2}$	1.0–160.0	7.0	19		0.992	1.069
	$^2\Pi_{3/2}$	3.0–160.0	7.0	19		1.118	1.025
	$^2\Sigma^+$	3.0–160.0	7.0	19		−1.544	1.633
	$^2\Sigma^+_{1/2}$	1.0–160.0	7.0	19		−1.800	1.842
	$^2\Sigma^+/^2\Pi$	1.0–160.0	7.0	21		0.531	0.689
	$^2\Sigma^+_{1/2}/^2\Pi_{1/2}/^2\Pi_{3/2}$	1.0–160.0	7.0	20		0.294	0.450
563 [13,14]	$^2\Pi$	1.0–40.0	5.0	17		0.714	0.734
	$^2\Pi_{1/2}$	1.0–40.0	5.0	15	0.1	0.491	0.531
	$^2\Pi_{3/2}$	1.0–40.0	5.0	16		0.705	0.725
	$^2\Sigma^+$	1.0–40.0	5.0	15	0.1	−3.863	3.863
	$^2\Sigma^+_{1/2}$	1.0–40.0	5.0	15	0.1	−4.359	4.378
	$^2\Sigma^+/^2\Pi$	1.0–40.0	5.0	17		−0.406	0.452
	$^2\Sigma^+_{1/2}/^2\Pi_{1/2}/^2\Pi_{3/2}$	1.0–40.0	5.0	16		−0.611	0.656

[a]A is the fractional accuracy of the experimental data and P is the fractional precision of the theoretical values. Where there is a blank entry in the P column, it implies that different precisions were used over different ranges, depending on the ease of convergence.

owing to the diffuseness of the orbitals, in fact the effect is minimal as far as the bond length and vibrational constants are concerned; the effect for the dissociation energies is of the order of 5%

In Fig. 2, the effect of "turning on" spin–orbit coupling is seen. In Fig. 2(a) we show the unperturbed $^2\Pi$ and $^2\Sigma^+$ states; in Fig. 2(b), we show the effect of spin–orbit coupling in the $^2\Pi$ state only (i.e., ignoring the presence of the $^2\Sigma^+$ state). The latter is modeled by assuming that the splitting for the $^2\Pi_{1/2}$ state is the same as that for the $^2\Pi_{3/2}$ state, but in the opposite direction. Figure 2(c) shows the effect of the interaction between the $^2\Pi_{1/2}$ and the $^2\Sigma^+_{1/2}$ states: the $^2\Pi_{1/2}$ state is pushed up in energy, so that it correctly approaches the $He+O^-(^2P_{1/2})$ asymptote, and the $^2\Sigma^+_{1/2}$ state is pushed down in energy, so that it correctly converges with the $^2\Pi_{3/2}$ state, approaching the $He+O^-(^2P_{3/2})$ asymptote. Since this repulsion is dependent upon the energetic separation, and since this separation depends upon the internuclear distance, the shapes of the two interacting curves also change during this interaction.

Considering first the $^2\Pi_{3/2}$ state, it may be seen from Table I that the results obtained for this state are essentially identical to those obtained for the unperturbed $^2\Pi$ state. There is little effect of the spin–orbit coupling for this state, except to move it down, parallel to the $^2\Pi$ curve. The $^2\Pi_{1/2}$ and $^2\Sigma^+_{1/2}$ states, on the other hand, change their shapes appreciably, with the $^2\Pi^+_{1/2}$ state becoming appreciably shallower than the unperturbed $^2\Sigma^+$ state. Concomitantly, the $^2\Pi_{1/2}$ state also becomes shallower upon interaction. Note that in the absence of the interaction with the $^2\Sigma^+_{1/2}$ state, the $^2\Pi_{1/2}$ state would be parallel to both the $^2\Pi_{3/2}$ state and the $^2\Pi$ state [see Fig. 2(b)], and consequently have the same R_e and vibrational constants. Consequently, we conclude that it is important to consider the effects of spin–orbit coupling in understanding the spectroscopy of the HeO^- ion.

2. Transport coefficients

Diffusion coefficients and mobilities have been calculated over wide ranges of E/N and at a variety of temperatures, and we have placed the results in the gaseous ion transport database at Chatham College.[28] Here, we will only discuss the mobility results since there have been no experimental determinations of diffusion coefficients. Of particular

importance here, and as noted above, is the fact that there are three low-lying spin–orbit states which can contribute, but the precise ratio to use is not clear.

In the HeO^- experiments of Viggiano, Morris, and Mason, the O^- ions were produced *via* electron impact on N_2O, in a relatively high-pressure regime (0.1–1 Torr). Although the distribution of the O^- states was not measured, it was speculated that the distribution was likely to have been statistical (i.e., 2:1 in favor of the $^2P_{3/2}$ state). Once interaction with He has occurred, assuming again that statistical behavior occurs, the appropriate ratio is 1:1:1 for the three spin–orbit states mentioned above.

The question naturally arises as to whether it is reasonable to assume statistical behavior, and essentially this implies two things. First, the production of the O^- ions is energetic enough that the higher energy $^2P_{1/2}$ state is produced with the same efficiency as the lower $^2P_{3/2}$ state. Second, that the populations remain statistical in the drift region (*vide infra*).

Let us now consider the statistics in Table II. These quantify the closeness of the agreement between the mobilities calculated using the potentials of the present work, and the smoothed experimental results[10,14] of Refs. 9 and 13. There are results presented for mobilities calculated using: each of the $^2\Sigma^+$ and $^2\Pi$ curves, i.e., ignoring spin–orbit coupling; for each of the three spin–orbit states, individually; for a 1:2 weighting of the $^2\Sigma^+$ and $^2\Pi$ curves, i.e., assuming statistical behavior in the absence of spin–orbit coupling; and finally a 1:1:1 weighting of the three spin–orbit states, i.e., assuming statistical behavior in the presence of spin–orbit coupling. In addition, in Fig. 3, we present a subset of these results graphically.

Considering first the results at 171 K, it may be seen that the results in the absence of spin–orbit coupling are quite reasonable for the $^2\Sigma^+$ state, but poor for the $^2\Pi$ state. The agreement is slightly better for the statistically weighted calculations. On moving to the calculations that employ the spin–orbit curves, it may be seen that the individual spin–orbit states do not give good agreement with experiment, with the results for the $^2\Sigma^+_{1/2}$ state being particularly poor. However, once a statistical weighting of the three spin–orbit states is employed, it may be seen that the agreement between theory and experiment is excellent.

Similar comments hold at 300 K, where the statistical weighting of the spin–orbit states gives the best agreement over the whole temperature range, with the final agreement being very good, as may be seen by eye in Fig. 3.

At 563 K, the picture is not so clear, with good agreement being obtained for the $^2\Pi$ states (with and without spin–orbit coupling), and good agreement being obtained for the statistical mixes (again, both with and without spin–orbit coupling). What is clear, is that the $^2\Sigma^+$ state on its own gives very poor agreement with experiment. What is more clear from Fig. 3 is that the calculated values lie consistently higher than the experimental ones (although at high E/N the calculated values come within the error bars). The indications are that the 563 K experimental mobilities are probably not reliable.

Finally, we consider the 93 K experiments. We first note

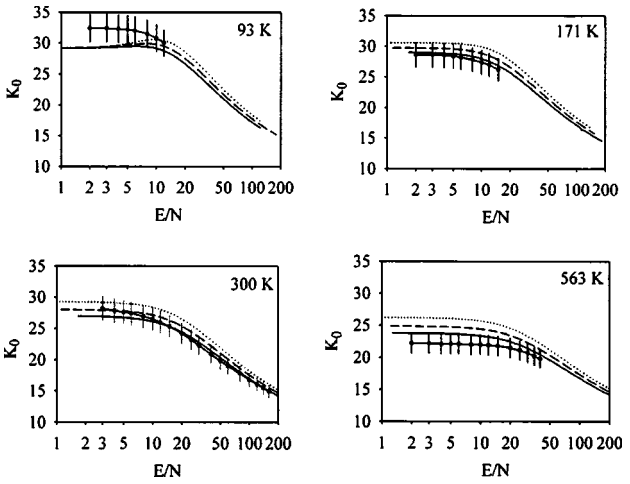

FIG. 3. Calculated standard mobilities ($cm^2\,V^{-1}\,s^{-1}$) for O^- in He as a function of E/N (*Td*) at different temperatures. The error bars indicate the estimated 7% experimental error, with the data being smoothed versions of the original experimental data set (see text for details and references). The solid line is for a statistical 1:1:1 ratio of the $^2\Sigma^+_{1/2}$, $^2\Pi_{3/2}$, and $^2\Pi_{1/2}$ states; the dashed line is for a corresponding 1:1:0 ratio; and the dotted line is for a 2:1:0 ratio.

that Viggiano, Morris, and Mason commented that these experimental results did not appear to fit in with those obtained at other temperatures. It is certainly the case that the agreement here, for all sets of calculations, was by far the worst, and, looking at Fig. 3, it is quite clear that the calculated mobilities are consistently lower than the experimental values, although at high E/N they come within the error bars. It should additionally be pointed out that the behavior of the experimental mobilities at 93 K is not as expected. The depth of the HeO^- $^2\Sigma^+_{1/2}$ well is $D_e = 75\ cm^{-1}$, which corresponds to thermal energy (k_BT) at a temperature of 108 K, and consequently one expects to see a distinct maximum in the mobility versus E/N curve at moderate E/N. This is indeed seen in the theoretical curves, but is absent in the 93 K experimental data. This again points to a problem with the data, as apparently suspected by Viggiano, Morris, and Mason.

What do these results imply about the experimental populations? Taken together, there seems to be little doubt that the best agreement between the experimental results and the calculations is found when a statistical weighting of the spin–orbit states is used. This is particularly the case at 171 K, and may also be seen fairly clearly with the 300 K results. Additional calculations (not reported here) with other weightings of the spin–orbit states gave results in greater disagreement with the experimental data than found for the statistical weighting. The conclusion is therefore that a statistical distribution of the $^2\Sigma^+_{1/2}$, $^2\Pi_{3/2}$, and $^2\Pi_{1/2}$ states was present in the experiments, and that changes in populations of these states through collisions happens at a rate that is infrequent enough not to affect the observed mobilities.

What is clear is that for a system such as O^- where energetically close states can contribute, then care must be taken when deciding what weighting of the contributing states needs to be employed in order to obtain agreement with experiment and/or provide accurate predictions of transport coefficients.

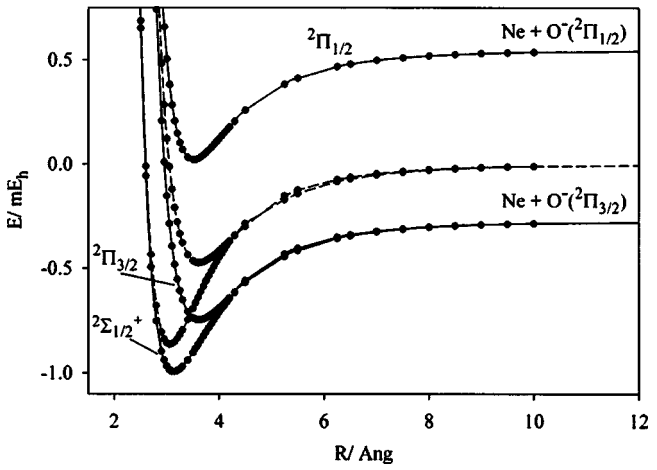

FIG. 4. RCCSD(T)/d-aug-cc-pV5Z curves for the $^2\Sigma^+$ and $^2\Pi$ states of NeO^- in the absence (dotted lines) and presence (solid lines) of spin–orbit coupling (see text for details).

B. NeO^-

In Fig. 4 are shown the $X\,^2\Sigma^+$ and $A\,^2\Pi$ potential energy curves for NeO^-, both in the absence and presence of spin–orbit coupling. Table III shows the derived spectroscopic constants for these curves. Considering first the spectroscopic parameters obtained with and without counterpoise correction, it may be seen that there is a change of ca. 5%–6% for the dissociation energies. This is similar in magnitude as for HeO^-, with again minimal changes to the bond length and vibrational constants. Again, this may be attributed to the rather long internuclear bond length, and the completeness of the basis set.

Moving on to the spin–orbit results, it may be seen that the constants of the $^2\Pi_{3/2}$ state are essentially identical with those of the $^2\Pi$ state. For the two $\Omega=1/2$ components, the interaction between them causes changes in the calculated parameters, and the curve shapes alter during the interaction. In particular we note that the $^2\Pi_{1/2}$ potential becomes slightly deeper, and steeper, with both of these being in line with an increased interaction as evinced also by the shorter bond length. Essentially the opposite trend happens for the $^2\Sigma^+$ state, which becomes more weakly bound as a result of the interaction.

The mobilities at 300 K are shown in Fig. 5, in addition to those for HeO^- and ArO^-.

C. ArO^-

Figure 6 shows our potential energy curves for the $X\,^2\Sigma^+$ and $A\,^2\Pi$ states of ArO^- both with and without spin–orbit coupling. Also shown are the non-spin–orbit curves of Buchachenko *et al.* A summary of the spectroscopic analysis of our curves, with and without counterpoise correction, and with and without spin–orbit effects is given in Table IV.

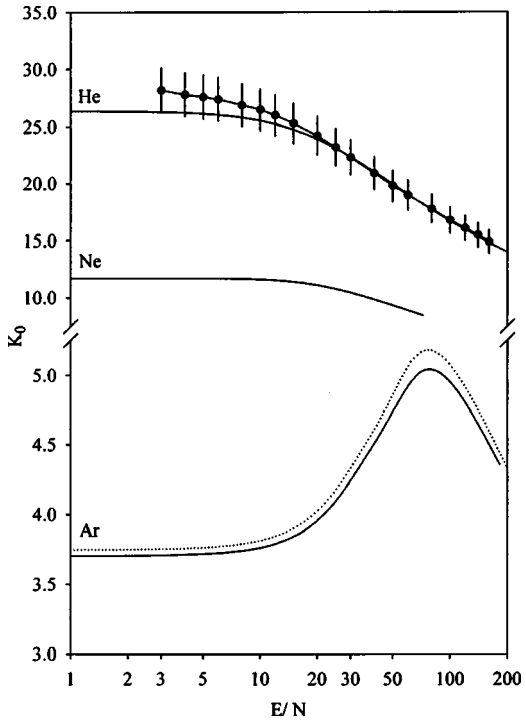

FIG. 5. Calculated standard mobilities ($cm^2\,V^{-1}\,s^{-1}$) for O^- in He, Ne, and Ar as a function of E/N (Td) at 300 K. The error bars for He indicate the estimated 7% experimental error, with the data being smoothed versions of the original experimental data set (see text for details and references). The dotted line for Ar represents the mobilities obtained using the spin–orbit curves obtained from Ref. 17. See text for details.

From Fig. 6 we note that our $^2\Sigma^+$ and $^2\Pi$ states are slightly deeper than those of Ref. 17 close to the minimum, but that there is excellent agreement at long R. This suggests that the difference between the two potentials is in the description of correlation energy, with the long-range electrostatics proving to be more facile to describe, as expected. The minima on the potential energy curve from Ref. 17 were found to be at 3.408 Å for the $^2\Pi$ state and 3.013 Å for the $^2\Sigma^+$ state. These both are in good agreement with the present values, as may be seen from both Table IV and Fig. 6. The well depths from Ref. 17 are 533 and 788 cm^{-1} for the corresponding states, which are somewhat smaller than for the present curves, as noted above. From Table IV, we note that the effect of counterpoise correction is relatively small for

TABLE III. Spectroscopic data derived for NeO^-.

State	CP	R_e (Å)	D_e (cm^{-1})	D_0 (cm^{-1})	ZPVE	0–1 (cm^{-1})	N_{vib}[a]
$^2\Sigma^+$	No	3.042	201.6	174.9	26.7	46.1	10
$^2\Sigma^+$	Yes	3.101	189.0	163.9	25.1	44.2	10
$^2\Sigma^+_{1/2}$	Yes	3.136	158.1	136.9	21.2	36.2	11
$^2\Pi$	No	3.585	110.9	94.9	16.0	27.3	9
$^2\Pi$	Yes	3.614	103.8	88.4	15.4	26.0	9
$^2\Pi_{3/2}$	Yes	3.613	103.8	88.4	15.4	26.9	9
$^2\Pi_{1/2}$	Yes	3.508	115.7	98.2	17.5	29.5	9

[a]Number of bound vibrational levels.

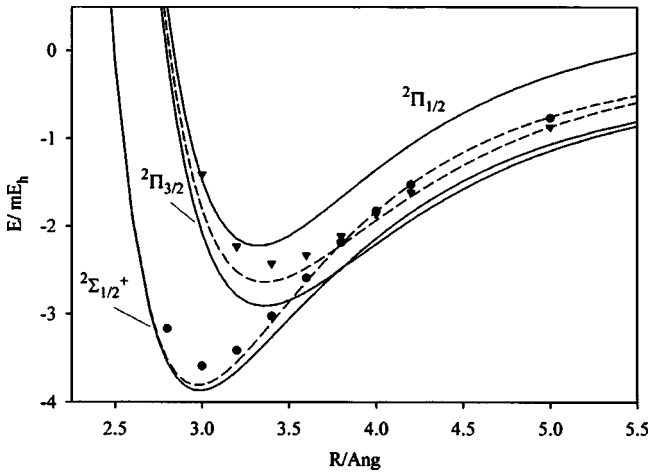

FIG. 6. Counterpoise-corrected RCCSD(T)/d-aug-cc-pV5Z curves for the $^2\Sigma^+$ and $^2\Pi$ states of ArO^- in the absence (dotted lines) and presence (solid lines) of spin–orbit coupling (see text for details). The results of Ref. 17 are represented as circles ($^2\Sigma^+$) and inverted triangles ($^2\Pi$)—see text for details.

both the internuclear distance and the vibrational constants. The effect on the dissociation energies is 16–17 cm^{-1}, but this amounts to only ~2%. Thus, even in ArO^-, which has the most polarizable Rg atom and diffuse orbitals of O^-, and for which we employed a slightly smaller basis set, the effect of basis set superposition error is very small.

The calculated parameters for the $^2\Pi_{3/2}$ state are reassuringly almost identical to those of the $^2\Pi$ state. As with the lighter two species, the two $\Omega=1/2$ states have their shapes affected by their interaction, with the $^2\Sigma_{1/2}^+$ state having a shallower potential, and the $^2\Pi_{1/2}$ state having a deeper potential, compared to the $^2\Sigma^+$ and $^2\Pi$ states, respectively.

As with the other two systems, we have calculated diffusion coefficients and mobilities. There are no experimental mobilities of O^- in Ar to which to compare, although first order mobilities[29] for O^- in Ar were calculated in Ref. 17. For those calculations the spin–orbit curves were employed, with a statistical ratio of the three spin–orbit states. For comparison to the results here, we constructed the spin–orbit energy points employing the UMP4 potential of Ref. 17, and employing the (corrected[29]) formulas in Eqs. (10) and (11) therein; these were then employed to calculate standard mobilities at 300 K to compare with our values. These are presented in Fig. 5, and values very close to those obtained in the present work are obtained, indicating that the potentials are somewhat similar, particularly at long R, as may be seen from Fig. 6.

IV. CONCLUSIONS

Accurate potential energy curves, including spin–orbit coupling, have been calculated for the three RgO^- species, HeO^-, NeO^-, and ArO^-. In all the three cases, the ground state is $^2\Sigma^+$ state, with $^2\Pi$ state lying higher in energy. The latter state is split by the spin–orbit interaction, essentially located on the oxygen, and the $\Omega=1/2$ component interacts with the $^2\Sigma_{1/2}^+$ state. These effects need to be included in order to obtain accurate spectroscopic constants, since we have shown that the constants obtained in the absence of spin–orbit coupling are significantly different. We have also seen that the effect of the counterpoise correction is quite small for these species, which is explained by the large basis set employed and the relatively large internuclear separation.

As noted in the Introduction, one of the most stringent tests of a potential energy curve is the ability to calculate mobilities accurately across a wide range of E/N. In the present case, experimental data was only available for HeO^-, and so we concentrated on this system in this paper. Although there may be some inaccuracies in some of the experimental data for HeO^-, we showed that for two parts of the data set (namely, those at 171 and 300 K), there was unambiguous proof that the best fit was from a statistical ratio of the spin–orbit states, suggesting that the experimental data resulted from such a ratio of states. In summary, very accurate potential energy curves have been obtained, and their accuracy appears to be maintained across a wide range of R, as adjudged by the good agreement with experimental mobilities across a wide range of E/N. We are therefore confident that the spectroscopic constants that have been derived are also accurate.

We conclude by noting that further measurements of the mobilities of O^- in He (and Ne and Ar) would be very useful; particularly those at low temperature and across a wide range of E/N. These would allow a better comparison between the calculated potentials and experiment. Spectroscopic measurements on the RgO^- species would also be useful, but are clearly challenging.

ACKNOWLEDGMENTS

The authors are grateful to the EPSRC for the award of computer time at the Rutherford Appleton Laboratories under the auspices of the Computational Chemistry Working Party (CCWP), which enabled these calculations to be performed. E.P.F.L. is grateful to the Research Grant Council (RGC) of the Hong Kong Special Administration Region

TABLE IV. Spectroscopic data derived for ArO^-.

State	CP	R_e (Å)	D_e (cm^{-1})	D_0 (cm^{-1})	ZPVE	0–1 (cm^{-1})	N_{vib}[a]
$^2\Sigma^+$	No	2.968	853.1	804.9	48.1	91.0	24
$^2\Sigma^+$	Yes	2.975	836.0	788.2	47.8	90.2	25
$^2\Sigma_{1/2}^+$	No	2.986	789.5	743.8	45.6	85.3	25
$^2\Pi$	No	3.352	594.0	559.1	34.9	65.8	23
$^2\Pi$	Yes	3.358	578.8	544.3	34.5	65.0	23
$^2\Pi_{3/2}$	Yes	3.358	578.7	544.1	34.6	65.2	23
$^2\Pi_{1/2}$	Yes	3.322	606.8	569.0	37.8	71.1	23

[a]Number of bound vibrational energy levels.

(HKSAR) and the Research Committee of the Hong Kong Polytechnic University for support. The work of L.A.V. was supported by the National Science Foundation. Dr. A. A. Buchachenko (Moscow State University) is thanked for useful discussions.

[1]P. Soldán, E. P. F. Lee, and T. G. Wright, J. Chem. Soc., Faraday Trans. **94**, 3307 (1998).
[2]P. Soldán, E. P. F. Lee, and T. G. Wright, Mol. Phys. **97**, 139 (1999).
[3]P. Soldán, E. P. F. Lee, J. Lozeille, J. N. Murrell, and T. G. Wright, Chem. Phys. Lett. **343**, 179 (2001).
[4]J. Lozeille, E. Winata, L. A. Viehland, P. Soldán, E. P. F. Lee, and T. G. Wright, Phys. Chem. Chem. Phys. **4**, 3601 (2002).
[5]J. Lozeille, E. Winata, L. A. Viehland, P. Soldán, E. P. F. Lee, and T. G. Wright, J. Chem. Phys. **119**, 3729 (2003).
[6]L. A. Viehland, J. Lozeille, P. Soldán, E. P. F. Lee, and T. G. Wright, J. Chem. Phys. **121**, 341 (2004).
[7]H. L. Hickling, L. A. Viehland, D. T. Shepherd, P. Soldán, E. P. F. Lee, and T. G. Wright, Phys. Chem. Chem. Phys. **6**, 4233 (2004).
[8]M. W. Chase, Jr., J. Phys. Chem. Ref. Data Monogr. **9** (1998).
[9]M. McFarland, D. L. Albritton, F. C. Fehsenfeld, E. E. Ferguson, and A. L. Schmeltekopf, J. Chem. Phys. **59**, 6610 (1973).
[10]H. W. Ellis, R. Y. Pai, E. W. McDaniel, E. A. Mason, and L. A. Viehland, At. Data Nucl. Data Tables **17**, 177 (1976).
[11]S. L. Lin and J. N. Bardsley, J. Chem. Phys. **66**, 435 (1977).
[12]V. L. Bychov, Teplofiz. Vys. Temp. **20**, 765 (1982) [in Russian].
[13]A. A. Viggiano, R. A. Morris, and E. A. Mason, J. Chem. Phys. **98**, 6483 (1993).
[14]L. A. Viehland and E. A. Mason, At. Data Nucl. Data Tables **60**, 37 (1995).
[15]S. T. Arnold, J. H. Hendricks, and K. H. Bowen, J. Chem. Phys. **102**, 39 (1995).
[16]H. L. de Clercq, J. H. Hendricks, and K. H. Bowen, J. Chem. Phys. **117**, 2619 (2002).
[17]A. A. Buchachenko, J. Jakowski, G. Chałasiński, M. M. Szczęśniak, and S. M. Cybulski, J. Chem. Phys. **112**, 5852 (2000).
[18]G. Chałasiński and M. M. Szczęśniak, Chem. Rev. (Washington, D.C.) **100**, 4227 (2000).
[19]C. Hampel, K. Peterson, and H.-J. Werner, Chem. Phys. Lett. **190**, 1 (1992).
[20]MOLPRO is a package of *ab initio* programs written by H.-J. Werner and P. J. Knowles, with contributions from J. Almlöf, R. D. Amos A. Berning *et al.*
[21]EMSL Basis Set Library {basis sets were obtained from the Extensible Computational Chemistry Environment Basis Set Database, Version 1/29/01, as developed and distributed by the Molecular Science Computing Facility, Environmental and Molecular Sciences Laboratory which is part of the Pacific Northwest Laboratory, P.O. Box 999, Richland, Washington 99352, USA, and funded by the U.S. Department of Energy. The Pacific Northwest Laboratory is a multiprogram laboratory operated by Battelle Memorial Institute for the U.S. Department of Energy under Contract No. DE-AC06-76RLO 1830. Contact David Feller or Karen Schuchardt for further information}.
[22]A. Berning, M. Schweizer, H.-J. Werner, P. J. Knowles, and P. Palmieri, Mol. Phys. **98**, 1823 (2000).
[23]R. J. LeRoy, LEVEL 7.2—a computer program for solving the radial Schrödinger equation for bound and quasibound levels, and calculating various expectation values and matrix elements (University of Waterloo Chemical Physics Research Program, Waterloo, 2000).
[24]L. A. Viehland, Comput. Phys. Commun. **142**, 7 (2001).
[25]L. A. Viehland, Chem. Phys. **70**, 149 (1982).
[26]L. A. Viehland, Chem. Phys. **179**, 71 (1994).
[27]L. A. Viehland, E. A. Mason, W. F. Morrison, and M. R. Flannery, At. Data Nucl. Data Tables **16**, 495 (1975).
[28]To access this database you must telnet to the computer named sassafrass.chatham.edu and logon as gastrans. The required password will be provided upon request by email to viehland@sassafrass.chatham.edu
[29]A. Buchachenko (private communication).